Noise-activated barrier crossing in multiattractor dissipative neural networks

Joseph D. Taylor,[1] Ashok S. Chauhan,[1] John T. Taylor,[2] Andrey L. Shilnikov,[3,4] and Alain Nogaret[1,*]
[1]*Department of Physics, University of Bath, Bath BA2 7AY, United Kingdom*
[2]*Department of Electronics and Electrical Engineering, University of Bath, Bath BA2 7AY, United Kingdom*
[3]*Neuroscience Institute, Georgia State University, Petit Science Center, 100 Piedmont Avenue Atlanta, Georgia 30303, USA*
[4]*Department of Mathematics and Statistics, Georgia State University, Petit Science Center, 100 Piedmont Avenue, Atlanta, Georgia 30303, USA*

(Received 3 December 2021; revised 20 March 2022; accepted 17 May 2022; published 6 June 2022)

Noise-activated transitions between coexisting attractors are investigated in a chaotic spiking network. At low noise level, attractor hopping consists of discrete bifurcation events that conserve the memory of initial conditions. When the escape probability becomes comparable to the intrabasin hopping probability, the lifetime of attractors is given by a detailed balance where the less coherent attractors act as a sink for the more coherent ones. In this regime, the escape probability follows an activation law allowing us to assign pseudoactivation energies to limit cycle attractors. These pseudoenergies introduce a useful metric for evaluating the resilience of biological rhythms to perturbations.

DOI: 10.1103/PhysRevE.105.064203

I. INTRODUCTION

Inhibitory neurons play an important part in the genesis of biological rhythms. They entrain long-range electrical activity in the brain [1] and produce the spatiotemporal signals that control motor actions [2,3]. A notable property of inhibitory networks is their ability to support coexisting modes of synchronized oscillations [4–8] evoked by sensory stimulation [9–11]. There is, however, a wide discrepancy between the number of oscillations theoretically predicted [8,12] and the relative paucity of experimentally observed ones [13–15]. This discrepancy might arise from different tolerances to noise among attractors [16]. Experiments on central pattern generators have shown that all limit cycle attractors survive mild noise levels and heterogeneity [11]; however, their stability at large noise levels is unknown. Experiments on crustacean central pattern generators have shown that biological rhythms only exist within a finite range of temperatures [17] and pH levels [18]. Outside of this range oscillations become arrhythmic. An objective metric is therefore needed for predicting the range of stability of biological rhythms.

In conservative systems (Hopfield networks [19], Boltzmann machines [20]), the robustness of attractors is defined by activation energies in a potential landscape representing bit configurations. The dissipative systems we are concerned with here (central pattern generators, the brain) do not have an equivalent potential landscape since the state is time dependent. Theoretical attempts have been made to describe interactions in terms of a time-independent function; however, a unifying theoretical description is yet to emerge. Graham and Tél [21,22] have introduced pseudopotentials; Stankovski *et al.* [23,24] multivariate coupling functions; while other researchers use phase-lag maps to visualize basins of attractions as an indirect effect of "potential wells" [4,5,11]. Attractor hopping is thus routinely analyzed in terms of bifurcations [25–28] rather than equilibrium thermodynamics. Dynamic networks and Hopfield network differ further in fundamental ways regarding their number of attractors and the sensitivity of these attractors to noise. Dynamic inhibitory networks host up to $(N-1)!/(\ln 2)^N$ attractors [11,12]. These are protected from noise by negative Lyapunov exponents [29,30]. In contrast, Hopfield networks [19] can in principle store 2^N states; however, the overlap of stored patterns limits this number to $0.14N$, a number that decreases exponentially with temperature [31]. Understanding the robustness of limit cycle attractors to noise requires demonstrating the existence of (i) an activation law, (ii) pseudoactivation energies and their relation to limit-cycle oscillations, and (iii) the reversibility or irreversibility of hopping events depending on whether it is controlled by fine-scale dynamics or thermodynamics.

Here, we answer these questions by measuring the noise-induced transitions between the six limit-cycle attractors of a three-neuron network. The network was implemented on a purposely built neuromorphic platform that integrates current stimuli with analog electronic circuits like those in the brain and that incorporate the same level of electronic noise and heterogeneity. Unlike in Chauhan *et al.* [11] where the initial state was chosen randomly in phase space, we have now prepared the network in a single attractor. We then varied the level of extrinsic noise over a range two orders of magnitude greater than Chauhan *et al.* to propel transitions out of this attractor. At low noise level, intrabasin transitions dominate. At intermediate noise level, the system hops into the state of immediately lower coherence. In this regime, the escape probability may be fitted with a Kramers-Arrhenius activation law [32,33]. At higher noise level, transitions skip the states of intermediate coherence to arrive into the most

*A.R.Nogaret@bath.ac.uk

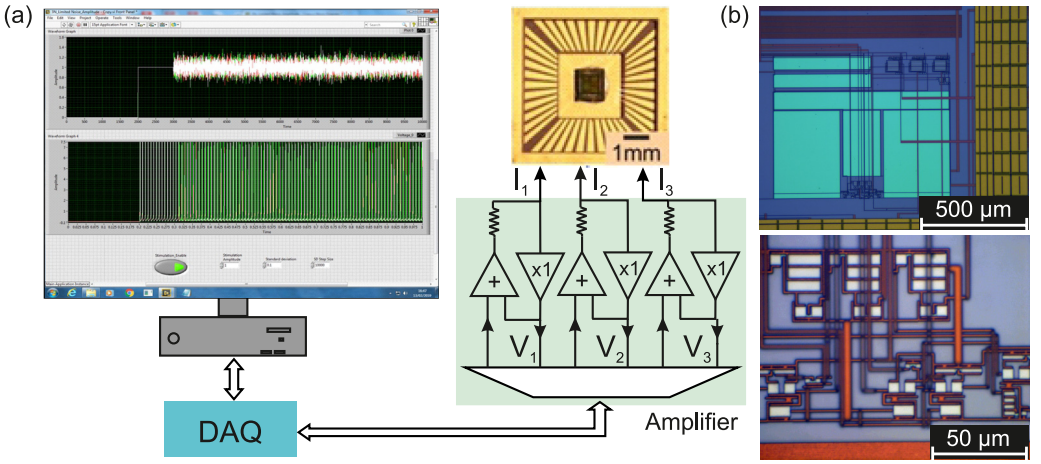

FIG. 1. Current-clamp measurements on a three-neuron network. (a) The current-clamp amplifier injects time series currents $I_1(t)$, $I_2(t)$, and $I_3(t)$ in the three-neuron network in the silicon chip and measures their voltage waveforms $V_1(t)$, $V_2(t)$, and $V_3(t)$. The prototypical current protocol is shown in the upper window of the computer screen. The 200-ms-long current step is followed by a 600-ms-long epoch where noise is added to propel transitions between attractors. The neuron oscillations are recorded in the lower window of the computer screen. (b) Micrograph of one neuron on the chip (top). Detail of an ion activation gate in 0.35 μm technology (bottom).

incoherent state. In this way we obtained the probability matrix of the Markov chain of the six attractors. We obtained the pseudoactivation energies of individual attractors and find they increase as the coherence of limit cycle oscillations decreases. Our demonstration of pseudoactivation energies in dissipative networks provides a simple metric for predicting the range of stability of network oscillations to perturbations [17,18].

II. EXPERIMENTAL METHOD

Noise-induced switching was simulated in a three-neuron network realized on a neuromorphic platform (Fig. 1). The network was made of Hogkin-Huxley NaKl neurons [34,35] interconnected with reciprocal inhibitory synapses [36]. The neurons were stimulated with delayed current steps $I_1(t)$, $I_2(t)$, and $I_3(t)$ synthesized by a current-clamp amplifier driven by a computer-controlled DAQ card [Fig. 1(a)]. Extrinsic Gaussian noise was synthesized using a pseudorandom number generator (Labview Gaussian White noise VI) and added to the current steps during an appropriate time window. The analog circuits on the chip integrated the current waveforms using the physical characteristics of semiconductor devices [Fig. 1(b)]. This had the advantage of integrating signals instantaneously, in continuous time, in the presence of residual electronic $1/f$ noise and component to component heterogeneity mimicking the intrinsic environment of the brain. The current-clamp amplifier picked up the voltage oscillations returned by the three neurons [Fig. 1(a)]. These were recorded by the computer. Both the neuron activation thresholds, neuron recovery time constants, ion channel conductances; and the synaptic threshold, synaptic decay time, and synaptic conductances were set by the gate voltages of field effect transistors [10,37]. Neurons had a 7 μA current threshold above which their oscillation frequency increased from 40 Hz at 8 μA to 300 Hz at 50 μA. The inhibitory postsynaptic current peaked at -12 μA and decayed with a time constant τ set between 1 and 4 ms. The period of neuron oscillations was $T = 14$ ms (20 μA). The synaptic threshold was set at 50% of the height of presynaptic action potentials to delay the onset of inhibition by $\approx$400 μs. This delay was essential to maximize the number of coexisting attractors by allowing coincident action potentials [10,11]. All neurons (respectively, synapses) were configured with the same nominal parameters.

The experiment was conducted in two steps covering consecutive time intervals 0–t_2 and t_2–t_3 in Fig. 2. The network was initially prepared in the chosen attractor during interval 0–t_2. Gaussian white noise was then added to current stimuli to induce attractor hopping (interval t_2–t_3). The network state was set in the basin of the initial attractor by choosing the current delays τ_{21}, τ_{31} that give the desired sequence of action potentials [Fig. 2(a)]. The initial momentum was imparted over one oscillation period since $0 < \tau_{23}, \tau_{31} < T$ (interval 0–t_1). The network state was then left to relax into the attractor state over the next 200 ms [interval (t_1–t_2) which was sufficient to absorb transient oscillations. The network has six basins representing all possible discharge sequences of neurons 1, 2, and 3 [Fig. 2(b)]. *Type C* represents action potentials discharging in clockwise, $1 \to 2 \to 3$, and anticlockwise $1 \to 3 \to 2$ sequences; *type B* are partially coherent sequences $1 \to \{2, 3\}$, $2 \to \{3, 1\}$, $3 \to \{1, 2\}$; *type A* is the coherent state $\{1, 2, 3\}$ with coincident action potentials. The five attractors and their basins are shown in the phase-lag maps plotting the dephasings of neurons 2 and 3 relative to neuron 1 (Φ_{21}, Φ_{31}) over intervals 0–t_2 in units of the oscillation period [Fig. 2(c)]. Once in the chosen attractor, Gaussian noise was applied over the next 600 ms to induce attractor switching (interval t_2–t_3). The final state of the network was recorded over the last oscillations of that time window and used to compute transition probabilities. The noise had a normal distribution $\mathcal{N}(0, \sigma)$. Its standard deviation was varied between $\sigma = 0$ and 300 mV. This covers a noise range 60 times greater than in Ref. [11]. High noise intensity was required to "depopulate" attractors. At $t > t_3$, current stimuli were reset ($I_{1-3} = 0$) for 200 ms to let the network return to its

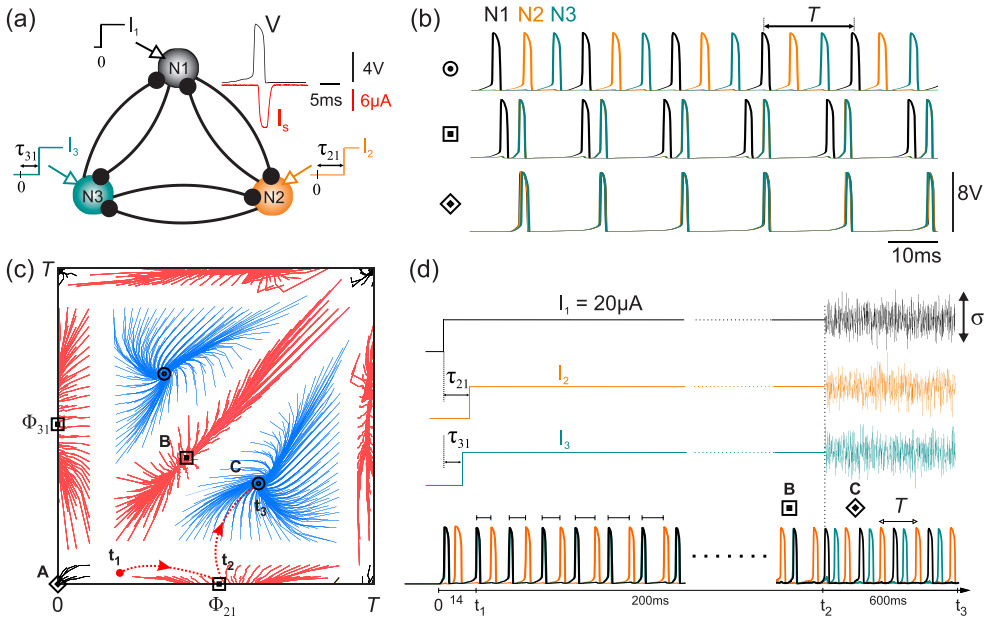

FIG. 2. Noise-activated switching between attractors. (a) Neurons N1, N2, and N3 interact via reciprocal inhibitory synapses. The timings of stimuli τ_{21} and τ_{31} set initial conditions. (b) The network has three types of synchronized oscillations: *type C* consists of sequential action potentials, *type B* consists of two coincident action potentials out of phase with the third, and *type A* has all three action potentials discharging simultaneously. (c) Phase-lag map plotting the trajectories of the network state $[\Phi_{21}(t), \Phi_{31}(t)]$ emanating from all possible initial states. $\Phi_{21}(t)$ and $\Phi_{31}(t)$ are the instantaneous dephasings of action potentials of neurons 2 and 3 relative to neuron 1 in units of the oscillation period T. (d) The network is prepared in a given state (B) by first placing it in the relevant basin of attraction (0–t_1), and letting it relax in the attractor (t_1–t_2). Noise is then applied to study transitions towards another attractor [t_2–t_3; arrows panel (c)].

quiescent state. The network state was then reinitialized and the noise level was incremented to probe the dependence of switch probabilities on noise for each attractor.

III. RESULTS

Figure 2(d) shows an example of noise-induced switching from the partially coherent state (B) to the sequential state (C). The switch occurs quasi-instantaneously in this example as the noise level is high ($\sigma = 300$ mV). Once the switch is complete, no reversion to the initial state occurs at any later point of the noise window t_2–t_3. For most practical purposes, the switch appears irreversible as we shall see below. This points to an activation process ruled by thermodynamics rather than reversible fine-scale dynamics.

A systematic study of escape probabilities out of the coherent state A and the partially coherent state B is shown in Figs. 3(a) and 3(b) as a function of noise. In Fig. 3(a), the *coherent state A* is stable up to $\sigma \approx 75$ mV where most noise-induced transitions are within the initial attractor basin. From $\sigma = 75$ mV to 230 mV a majority of transitions terminate in the partially coherent states B as the number of intrabasin transitions rapidly decreases. It is noteworthy that outbound transitions end up preferentially in either one of the three partially coherent states (B) rather than the two incoherent states (C). It is only from $\sigma \approx 230$ mV and above that hopping from the coherent state occurs directly into the incoherent states without transitioning through the partially coherent states. This suggests that noise activated hopping follows a sequential process trickling down the coherence order into states of lower and lower coherence as the noise amplitude increases. Turning to Fig. 3(b), intrabasin transitions similarly dominate at low noise until $\sigma \approx 230$ mV. Reverse switching events from the partially coherent state towards the coherent state are negligible in comparison to intrabasin transitions and are therefore not visible. When $\sigma > 230$ mV the network switches out of the partially coherent attractor into incoherent states (C). Note the absence of significant reverse switching into the coherent state (A) or into the other two partially coherent attractors (B) [Fig. 3(b)]. This apparent irreversibility where the incoherent states act as a sink for the more coherent states suggests that a thermodynamic equilibrium is reached at higher noise levels and that the lifetime of attractors is given by a detailed balance of transitions.

Noise carries a power per unit bandwidth which is dissipated across the leak resistance of the neuron membrane ($R = 50\ k\Omega$). The power spectral density is equivalent to a thermal energy as prescribed by Johnson and Nyquist [38,39]:

$$\frac{\sigma^2}{R\Delta f} = 4k_B T, \tag{1}$$

where Δf is a unit of noise bandwidth, k_B is Boltzmann's constant, and T is the temperature of the reservoir. Noise therefore provides a reservoir with its own energy and entropy in equilibrium with the discernible microstate states of the network. These microstates are the state trajectories differentiated by their initial conditions [Fig. 2(c)]. The microstates are assumed to be equiprobable and their number to be very large. For the network at equilibrium, the most likely macrostate will be the state of maximum disorder with a probability that depends exponentially on temperature $P = \exp(-E/k_B T)$ where E has the dimension of an energy.

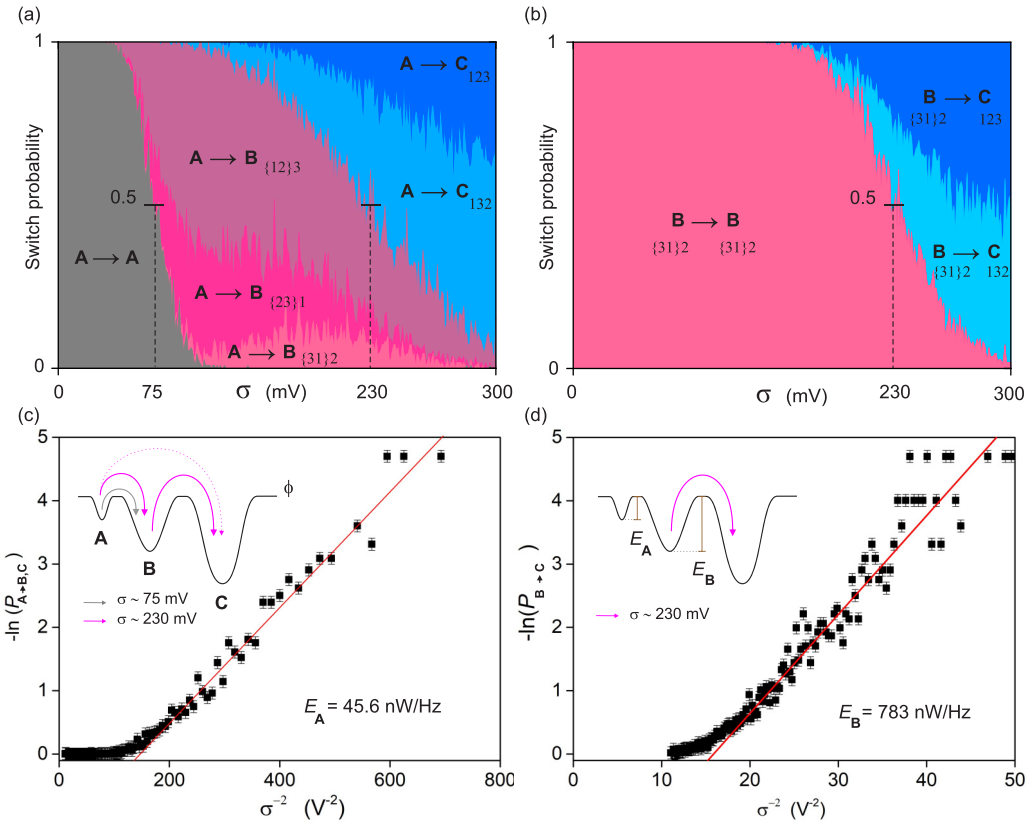

FIG. 3. Detailed balance of transitions between attractors. (a) Probabilities of transition from the coherent state (A) towards any of the other five attractors and to self, as a function of noise. (b) Probabilities of transition from the partially coherent state (B) towards any of the five other attractors and to self. (c) Escape probability out of A as a function of noise, fitted with Eq. (2) (red line). Inset: noise-activated hopping in the nonequilibrium potential, ϕ, showing capture by the final state B at moderate noise (∼75 mV) and by final state C at $\sigma \sim 230$ mV. When $\sigma < 230$ mV hopping into C is a sequential process that occurs via B (full purple arrows). When $\sigma > 230$ mV, hopping into C is direct (dashed purple arrow). (d) Escape probability out of B as a function of noise.

Substituting k_BT with the variance of noise using Eq. (1), the probability of the macrostate is

$$P = \exp\left(-\frac{4R\Delta f E}{\sigma^2}\right). \tag{2}$$

In order to test this picture we have plotted the noise-induced escape probability from the initial attractor as a function of the inverse of the noise variance. This is shown in Fig. 3(c) for the coherent attractor ($P_{A\to B,C}$) and in Fig. 3(d) for the partially coherent attractor ($P_{B\to C}$). In the limit of high noise levels ($\sigma^{-2} \to 0$), the escape probability approaches unity. As noise gradually decreases and approaches the 75 and 230 mV thresholds, the escape probability decreases exponentially with the inverse of the noise variance, validating Eq. (2). A least-square fit of the probability data (red line) gives pseudoactivation energies of $E_A = 45.6$ nW/Hz for the coherent attractor and $E_B = 783$ nW/Hz for the partially coherent attractor. As the noise amplitude decreases below these thresholds, the statistical sample of events used to calculate the escape probability becomes very small. This gives a wider dispersion of escape probabilities in Figs. 3(c) and 3(d).

The detailed balance of transitions between attractors is consistent with the existence of a pseudopotential similar to that plotted in the insets to Figs. 3(c) and 3(d). The pseudoactivation energies define the depth of pseudopotential wells. When the noise variance is small compared to the activation energy, transitions take place within the initial well. When noise increases to become comparable to the pseudoactivation energy, transitions in and out of the initial attractor erase the memory of initial conditions and a detailed balance is established. The detailed balance assigns exponentially small lifetimes to the more coherent states: $\tau_{A,B}/\tau_C = \exp[-4R\Delta f(E_C - E_{A,B})/\sigma^2]$. The occupancy of the coherent state τ_B/τ_A remains very small over a wide range due to the large difference in pseudoactivation energies. For example, at $\sigma = 75$ mV, $\tau_A/\tau_B = 4 \times 10^{-12}$, which explains why reverse switching into the coherent state is never observed [Fig. 3(a)]. The detailed balance also explains the sequential activation of transitions into attractors of increasingly low coherence as noise increases [Fig. 3(a)]. The partially coherent attractors initially act as a sink to the coherent attractor [Fig. 3(c), gray arrow]. This only lasts until noise is sufficient to overcome the pseudoactivation energy of the partially coherent attractor, at which point the incoherent attractors become the new sink [Figs. 3(c) and 3(d), purple arrows]. This sink is with respect to both the partially coherent attractor selected by current stimuli and the two equivalent attractors (B). This is why transitions $\{3,1\}2 \Rightarrow \{1,2\}3$ and $\{3,1\}2 \Rightarrow \{2,3\}1$ are not observed in Fig. 3(b).

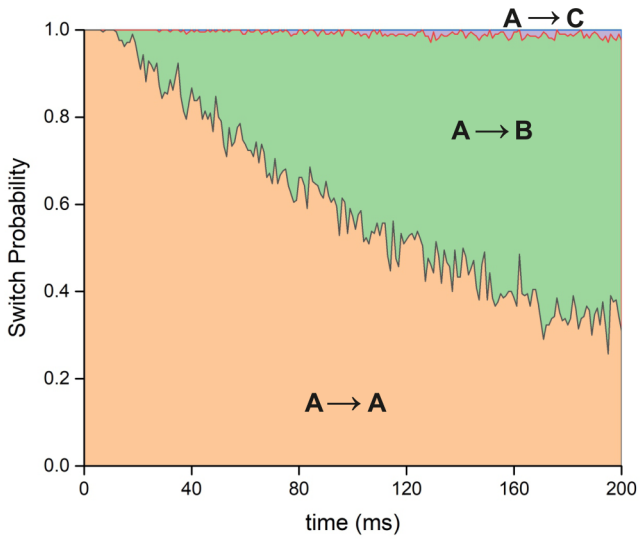

FIG. 4. Temporal dependence of the switching probability out of the coherent state A. Noise of amplitude $\sigma = 100$ mV is applied at $t = 10$ ms.

We have also measured the time dependence of the switch probability from the instant that noise was applied to determine the instantaneous switch rates (Fig. 4). Under a noise level of $\sigma = 100$ mV, the occupancy of the initial state decays exponentially over the first 200 ms. The rate of escape increases exponentially as noise amplitude increases and at $\sigma = 300$ mV, switching is almost instantaneous [Fig. 2(d)].

IV. DISCUSSION

Our neural hardware models the equations of motion of neurons and synapses [40] in the presence of $1/f$ electronic noise and component-to-component heterogeneity. The system integrates 18 coupled differential equations (4×3 neurons + 6 synapses) to compute the network state. Unlike conservative systems [19,20] this state does not have a time-independent energy function. Limit-cycle attractors [5,8,10] are sequences of action potentials rather than local minima of an energy function representing bit configurations. In dissipative systems, attractor switching is analyzed in dynamic terms of bifurcations, event timing, initial conditions, and the realizations of noise [25–27]. In conservative systems attractor hopping follows equilibrium thermodynamics [41].

Our experiments on noise-activated switching distinguish a low noise regime dominated by intrabasin transitions and a higher noise regime not investigated previously where 50% or more transitions are interattractor transitions. In the low noise regime, state trajectories conserve the memory of initial conditions and interdiffuse reversibly between attractor basins [11]. The escape probability cannot be defined over our finite 600 ms interval and has the broad distribution seen in Figs. 3(c) and 3(d) at $\sigma \to 0$. In the high noise regime, single event dynamics is replaced with the detailed balance of transitions between attractors. The state at the end of the 600-ms observation window is determined with greater consistency and the escape probability in Figs. 3(c) and 3(d) narrows down on the exponential trend line (red line). The memory of initial conditions is lost. The attractor lifetime is now given by the detailed balance of transitions. Pseudoactivation energies validate the hypothesis of pseudopotential barriers made by Graham and Tél [21,22] in dissipative multiattractor neural networks.

The detailed balance principle explains the transition probabilities reported in Figs. 3(a) and 3(b) and their dependence on noise. These together with the remaining transitions with vanishingly small probabilities give the Markov transition matrix of the six-attractor system. Hopping is effectively unidirectional from coherent to incoherent attractors. Reverse transitions from the incoherent to the coherent states have a very low probability due to the different pseudoactivation energies and vanishing lifetime of the coherent attractor. Hopping among attractors of the same type [e.g., B in Fig. 3(b)] is improbable because these transitions compete with transitions into attractors of lower coherence. The attractor of lowest coherence whose pseudoactivation energy is greater than the noise variance will act as a sink for all transitions emanating from states of higher coherence. Asymmetrical hopping probabilities into the three B states in Fig. 3(a) is likely due to residual imbalance in the network connectivity. Preferential noise-induced hopping is known to occur in multistable dynamical systems [25]. We have also investigated noise-induced switching in a four-neuron network building on the low noise work of Chauhan *et al.* [11]. The same detailed balance is established at higher noise level as in the present three-neuron network. This now takes place between 24 attractors. The coherent attractor, in particular, is less stable than in the three-neuron network.

The pseudoactivation energies of dissipative dynamic networks are likely to have several important applications. They are easy to compute and will be important to estimate the range of stability of oscillations to perturbations other than noise that may be quantified in terms of an energy, such as temperature [17] and pH [18]. The broad distribution of pseudoactivation energies in multiattractor networks will further explain the discrepancy between the plethora of theoretically predicted attractors and the smaller number observed in biological networks. Lastly, our work paves the way to engineering the pseudopotentials of dissipative networks to solve computationally hard problems in the same way as the free energy of Hopfield-like conservative networks and is optimized to perform integer factorization [42] or simulated annealing [41,43]. Wojcik *et al.* [5] and Schwabedal *et al.* [44] have shown that the size and location of attractor basins may be tuned with the network connectivity. If used in this way it is expected that dynamical networks would hold many more information patterns for their larger number of attractors $[(N-1)!/(ln2)^N$ against $2^N]$ which are protected from noise.

The advantages and limitations of neuromorphic hardware as a test bench for nonlinear dynamics are as follows. The development of neuromorphic models is driven by bioelectronic medicine, in particular cardiac pacing [45], where they provide effective solutions [46] and brain-machine interfaces [47]. Applications aside, both analog neuron models [40,48] and computational models [49,50] are equally capable of predicting the state of a biological neuron to near perfection when configured with the right parameters. Both types of models are thus equally suited to modeling functional biocircuits. It should also be noted that all neuron models are guesses

irrespective of whether they are hardware or computational models. Model error is currently the major hurdle for estimating meaningful biological parameters. Parameter estimation frequently assigns erroneous values to parameter solutions to compensate for model error when fitting electrophysiological data. Neuromorphic computation has the advantage of being instantaneous, accurate, and free from approximations although it requires a time investment to build the hardware. Nonideal situations are modeled by default including device-specific heterogeneity, $1/f$ electric noise with multiple sources distributed across the spatial structure of the network. Probing the dynamics of actual living cells would be an ideal alternative; however, it would require isolating a functional subnetwork, injecting multiple stimuli and recording multiple neurons simultaneously without cross-talk. Any of these undertakings, on its own, is beyond current experimental capabilities in electrophysiology. Assuming a functional network could be isolated and measured, the lack of knowledge on electrochemical parameters [51] (neuromodulation, ion pumps...) would add uncertainty to the recorded data. Until experimental methods in neuroscience are sufficiently advanced to probe network dynamics in vitro, neuromorphic hardware will provide a powerful proxy for testing concepts in nonlinear dynamics free from uncertainty in electrical characteristics.

V. CONCLUSION

Our experiments unify the theoretical picture of time-independent interactions in dissipative dynamical systems by validating the existence of pseudopotentials. Unlike conservative systems where the free energy exists independently of noise, the pseudopotential barriers of our dissipative dynamical network form when the escape probability becomes comparable to the intrabasin hopping probability. When the noise level is low, attractor switching occurs through small-scale bifurcation events. We have obtained the pseudoactivation energies of limit-cycle attractors and show that these energies increase rapidly with the incoherence of synchronized oscillations. This energy-based metric is important to predict the range of stability of biological rhythms to perturbations (thermal, electrochemical, pressure) that may be expressed as energies.

ACKNOWLEDGMENTS

This work was supported by the European Union's Horizon 2020 Future Emerging Technologies Programme under Grant No. 732170.

[1] M. Bartos, I. Vida, and P. Jonas, Synaptic mechanisms of synchronized gamma oscillations in inhibitory interneuron networks, Nat. Rev. Neurosci. **8**, 45 (2007).

[2] A. I. Selverston, Invertebrate central pattern generator circuits, Philos. Trans. R. Soc. B **365**, 2329 (2010).

[3] E. Marder and D. Bucher, Central pattern generators and the control of rhythmic movements, Curr. Biol. **11**, R986 (2001).

[4] C. C. Canavier, D. A. Baxter, J. W. Clark, and J. H. Byrne, Control of multistability in ring circuits of oscillators, Biol. Cybern. **80**, 87 (1999).

[5] J. Wojcik, J. Schwabedal, R. Clewley, and A. Shilnikov, Key bifurcations of bursting polyrhythms in 3-cell central pattern generators, PLoS ONE **9**, e92918 (2014).

[6] D. Huber and L. S. Tsimring, Dynamics of an Ensemble of Noisy Bistable Elements with Global Time Delayed Coupling, Phys. Rev. Lett. **91**, 260601 (2003).

[7] R. C. Elson, A. I. Selverston, H. D. I. Abarbanel, and M. I. Rabinovich, Inhibitory synchronization of bursting in biological neurons: Dependence on synaptic time constant, J. Neurophysiol. **88**, 1166 (2002).

[8] M. Rabinovich, A. Volkovskii, P. Lecanda, R. Huerta, H. D. I. Abarbanel, and G. Laurent, Dynamical Encoding by Networks of Competing Neuron Groups: Winnerless Competition, Phys. Rev. Lett. **87**, 068102 (2001).

[9] M. I. Rabinovich, P. Varona, A. Selverston, and H. D. I. Abarbanel, Dynamical principles in neuroscience, Rev. Mod. Phys. **78**, 1213 (2006).

[10] A. S. Chauhan, J. D. Taylor, and A. Nogaret, Dual mechanism for the emergence of synchronization in inhibitory neural networks, Sci. Rep. **8**, 11431 (2018).

[11] A. S. Chauhan, J. D. Taylor, and A. Nogaret, Local inhibitory networks support up to $(n-1)!/(ln2)^n$ limit cycles in the presence of noise and heterogeneity, Phys. Rev. Research **3**, 043097 (2021).

[12] A. Nogaret and A. King, Inhibition delay increases neural network capacity through Stirling transform, Phys. Rev. E **97**, 030301(R) (2018).

[13] J. Jing and R. Gillette, Central pattern generator for escape mechanism in the notaspid sea slug: *Pleurobranchea californatica*, J. Neurophysiol. **81**, 654 (1999).

[14] P. A. Getting, A network oscillator underlying swimming in Tritonia, *Neuronal and Cellular Oscillators* (Marcel Dekker, Inc., New York, 1989), pp. 215–236.

[15] J. E. Rubin, N. A. Shevtsova, G. B. Ermentrout, J. C. Smith, and I. A. Rybak, Multiple rhythmic states in a model of the respiratory central pattern generator, J. Neurophysiol. **101**, 2146 (2009).

[16] A. A. Faisal, L. P. J. Selen, and D. M. Wolpert, Noise in the nervous system, Nat. Rev. Neurosci. **9**, 292 (2008).

[17] L. S. Tang, A. L. Taylor, A. Rinberg, and E. Marder, Robustness of a rhythmic circuit to short- and long-term temperature changes, J. Neurosci. **32**, 10075 (2012).

[18] J. A. Haley, D. Hampton, and E. Marder, Two central pattern generators from the crab: Cancer Borealis respond robustly and differentially to extreme extracellular pH, eLife **7**, e41877 (2018).

[19] J. J. Hopfield, Neural networks and physical systems with emerging collective computational abilities, Proc. Natl. Acad. Sci. USA **79**, 2554 (1982).

[20] D. H. Ackley, G. E. Hinton, and T. J. Sejnowski, A learning algorithm for Boltzmann machines, Cognit. Sci. **9**, 147 (1985).

[21] R. Graham and T. Tél, Existence of a Potential for Dissipative Dynamical Systems, Phys. Rev. Lett. **52**, 9 (1984).

[22] R. Graham and T. Tél, Nonequilibrium potential for coexisting attractors, Phys. Rev. A **33**, 1322 (1986).
[23] T. Stankovski, T. Pereira, P. V. E. McClintock, and A. Stefanovska, Coupling functions: Universal insights into dynamical interaction mechanisms, Rev. Mod. Phys. **89**, 045001 (2017).
[24] T. Stankovski, T. Pereira, P. V. E. McClintock, and A. Stefanovska, Coupling functions: Dynamical interaction mechanisms in the physical, biological and social sciences, Philos. Trans. A **377**, 20190039 (2019).
[25] S. Kraut, U. Feudel, and C. Grebogi, Preference of attractors in noisy multistable systems, Phys. Rev. E **59**, 5253 (1999).
[26] S. Kraut and U. Feudel, Multistability, noise, and attractor hopping: The crucial role of chaotic saddles, Phys. Rev. E **66**, 015207(R) (2002).
[27] P. Channell, I. Fuwape, A. B. Neiman, and A. L. Shilnikov, Variability of bursting patterns in a neuron model in the presence of noise, J. Comput. Neurosci. **27**, 527 (2009).
[28] D. S. Goldobin and A. Pikovsky, Antireliability of noise-driven neurons, Phys. Rev. E **73**, 061906 (2006).
[29] D. S. Goldobin and A. Pikovsky, Synchronization and desynchronization of self-sustained oscillators by common noise, Phys. Rev. E **71**, 045201(R) (2005).
[30] H. Nakao, Phase reduction approach to synchronisation of nonlinear oscillators, Contemp. Phys. **57**, 188 (2016).
[31] D. J. Amit, H. Gutfreund, and H. Sompolinsky, Storing Infinite Numbers of Patterns in a Spin-Glass Model of Neural Networks, Phys. Rev. Lett. **55**, 1530 (1985).
[32] H. A. Kramers, Brownian motion in a field of force and the diffusion model of chemical reactions, Physica **7**, 284 (1940).
[33] P. Hänggi, P. Talkner, and M. Borkovec, Reaction rate theory: Fifty years after Kramers, Rev. Mod. Phys. **62**, 251 (1990).
[34] A. L. Hodgkin and A. F. Huxley, A quantitative description of membrane current and its application to conduction and excitation nerve, J. Physiol. **117**, 500 (1952).
[35] M. Mahowald and R. Douglas, A silicon neuron, Nature (London) **354**, 515 (1991).
[36] C. Bartolozzi and G. Indiveri, Synaptic dynamics in analog VLSI, Neural Comput. **19**, 2581 (2007).
[37] L. Zhao and A. Nogaret, Experimental observation of multistability and dynamic attractors in silicon central pattern generators, Phys. Rev. E **92**, 052910 (2015).
[38] J. Johnson, Thermal agitation of electricity in conductors, Phys. Rev. **32**, 97 (1928).
[39] H. Nyquist, Thermal agitation of electric charge in conductors, Phys. Rev. **32**, 110 (1928).
[40] K. Abu-Hassan, J. D. Taylor, P. G. Morris, E. Donati, Z. A. Bortolotto, G. Indiveri, J. F. R. Paton, and A. Nogaret, Optimal solid state neurons, Nat. Commun. **10**, 5309 (2019).
[41] S. Kirkpatrick, Jr., C. D. Gelatt, and M. P. Vecchi, Optimization by simulated annealing, Science **220**, 671 (1983).
[42] W. A. Borders, A. Z. Pervaiz, S. Fukami, K. Y. Camsari, H. Ohno, and S. Datta, Integer factorization using stochastic magnetic tunnel junctions, Nature (London) **573**, 390 (2019).
[43] N. Metropolis, A. E. Rosenbluth, M. N. Rosenbluth, A. H. Teller, and T. Edward, Equation of state calculations by fast computing machines, J. Chem. Phys. **21**, 1087 (1953).
[44] J. T. C. Schwabedal, A. B. Neiman, and A. L. Shilnikov, Robust design of polyrhythmic circuits, Phys. Rev. E **90**, 022715 (2014).
[45] A. Nogaret, E. L. O'Callaghan, R. M. Lataro, H. C. Salgado, C. D. Meliza, E. Duncan, H. D. I. Abarbanel, and J. F. R. Paton, Silicon central pattern generators for cardiac diseases, J. Physiol. **593**, 763 (2015).
[46] J. Shanks, Y. Abukar, N. A. Lever, M. Pachen, I. J. LeGrice, D. J. Grossman, A. Nogaret, J. F. R. Paton, and R. Ramchandra, Reverse re-modelling chronic heart failure by reinstating heart rate variability, Basic Res. Cardiol. **117**, 4 (2022).
[47] E. Musk and Neuralink, An integrated brain-machine interface platform with thousands of channels, J. Med. Internet Res. **21**, e16194 (2019).
[48] J. Wang, D. Breen, A. Akinin, F. Broccard, and H. D. I. Abarbanel, Assimilation of biophysical neuronal dynamics in neuromorphic VLSI, IEEE Trans. Biomed. Circuits Syst. **11**, 1258 (2017).
[49] C. D. Meliza, M. Kostuk, H. Huang, A. Nogaret, D. Margoliash, and H. D. I. Abarbanel, Estimating parameters and predicting membrane voltages with conductance-based neuron models, Biol. Cybern. **108**, 495 (2014).
[50] A. Nogaret, C. D. Meliza, D. Margoliash, and H. D. I. Abarbanel, Automatic construction of predictive neuron models through large scale assimilation of electrophysiological data, Sci. Rep. **6**, 32749 (2016).
[51] T. O'Leary, A. C. Sutton, and E. Marder, Computational models in the age of large datasets, Curr. Opin. Neurobiol. **32**, 87 (2015).